Rock Mechanics and Rock Engineering (2022) 55:7289–7306
https://doi.org/10.1007/s00603-022-03030-3

ORIGINAL PAPER

Prediction of Mode I Fracture Toughness of Shale Specimens by Different Fracture Theories Considering Size Effect

Qin Xie[1] · Xiling Liu[1] · Shengxiang Li[1] · Kun Du[1] · Fengqiang Gong[2] · Xibing Li[1]

Received: 12 October 2021 / Accepted: 4 August 2022 / Published online: 4 September 2022

Abstract

In this study, mode I fracture tests on cracked straight-through Brazilian disc (CSTBD) and notched semi-circular bend (NSCB) shale specimens with different sizes were conducted to investigate the difference between maximum tangential stress fracture criterion and the size effect law (SEL) model in predicting apparent fracture toughness (K_a) of shale. In addition, the effects of specimen size and geometry on the K_a and the selection of fracture criterion on the prediction of the inherent fracture toughness (K_{Ic}) were also studied. The results show that the K_a increases with the increase of specimen size, and the difference between K_{Ic} of shale specimens with different sizes predicted by the fracture process zone length determined by the further improved maximum tangential stress (FIMTS) criterion is the smallest. For the prediction of K_a of NSCB specimen, the results predicted by the FIMTS criterion are the closest to the tested fracture toughness. However, the effect of SEL model applied to the prediction of K_a of NSCB specimens is poor. The effective establishment of SEL model requires high accuracy for test data, especially for the configuration with large variation of the dimensionless stress intensity factor (Y^*) with normalized crack length (α).

Highlights

- Fracture toughness is closely related to the size and configuration of the specimen, which is ultimately attributed to the inconsistent tangential stress distribution at the crack tip.
- The further improved maximum tangential stress criterion has the best effect on apparent fracture toughness prediction, and higher-order terms of the Williams expansion should be considered in apparent fracture toughness prediction of small-size specimens.
- The fracture criterion for determining the fracture process zone length should be consistent with the prediction criterion of apparent fracture toughness.
- The effective establishment of size effect law requires high accuracy tested data, especially for the configuration with large variation of the dimensionless stress intensity factor with normalized crack length.

Keywords Fracture toughness · Fracture process zone (FPZ) · Fracture criterion · Size effect law (SEL) · Cracked straight-through Brazilian disc (CSTBD) · Notched semi-circular bend (NSCB)

Abbreviations

$A_1, A_2, A_3, \ldots, A_n, B_n$	Coefficients of the crack tip asymptotic field
$A_{1c}, A_{2c}, A_{3c}, \ldots, A_{nc}$	Critical coefficients of the crack tip asymptotic field
a	Half of crack length for CSTBD or crack length for NSCB
a_{ec}	Effective crack length
B	Specimen thickness
BDT	Brazilian disc test

✉ Xiling Liu
lxlenglish@163.com

[1] School of Resources and Safety Engineering, Central South University, Changsha 410083, Hunan, China

[2] School of Civil Engineering, Southeast University, Nanjing 211189, China

CSTBD	Cracked straight-through Brazilian disc
CCNBD	Cracked chevron notched Brazilian disc
CB	Chevron bend
CNSCB	Chevron notch semi-circular bend
COD	Crack opening displacement
c	Critical distance from crack tip
c_f	Reference length
D	Specimen diameter
DCR	Diametrally compressed ring
DIC	Digital image correlation
NSCB	Notched semi-circular bend
E	Elastic modulus
ECT	Edge cracked triangular
ENDB	Edge-notched disc bend
ENDC	Edge-notched diametrically compressed disc
f_t	Tensile strength
FBD	Flattened Brazilian disc
FEM	Finite-element model
FIMTS	Further improved maximum tangential stress
FPZ	Fracture process zone
$g(\alpha)$	Dimensionless energy release rate
$g'(\alpha)$	Derivative of dimensionless energy release rate
G_f	Fracture energy of material
$G(\alpha)$	Energy release rate
ISRM	International Society for Rock Mechanics
$k(\alpha)$	Dimensionless functions
K_a	Apparent fracture toughness
K_I	Mode I stress intensity factor
K_{Ic}	Inherent fracture toughness
L	Characteristic length
LEFM	Linear elastic fracture mechanics
MMTS	Modified maximum tangential stress
n	The ordinal number of a term
NSCB	Notched semi-circular bend
P	Load on specimen
P_{max}	Maximum loading force
R	Specimen radius
r	Distance from the crack tip
r_c	Fracture process zone length
S	Half of support span
SCB	Semi-circular bend
SECRBB	Single edge crack round bar bending
SEL	Size effect law
SR	Short rod
TMTS	Traditional maximum tangential stress
VNSRB	V-notched short rod bend
VDM	Virtual displacement meter
Y^*	Dimensionless stress intensity factor
α	Normalized crack length
α_0	Normalized initial crack length
α_{ec}	Normalized effective crack length
θ	Direction of fracture in polar coordinates
$\sigma_{\theta\theta}$	Tangential stress
σ_x, σ_y, σ_z	Stresses
σ_N	Nominal stress
σ_{Nu}	Nominal failure stress

1 Introduction

With the continuous exploitation of conventional resources, oil and gas resources with the characteristics of centralized storage and easy exploitation are decreased sharply, and the exploitation of unconventional oil and gas resources is gradually highlighted. As an important means for oil and gas well stimulation, hydraulic fracturing has been widely used in the exploitation of shale gas and shale oil. The main principle of hydraulic fracturing to increase shale gas production is to create fractures perpendicular to the direction of minimum principal stress in the low-permeability strata and eventually through the production formation. The initiation and propagation of cracks in low-permeability strata are largely dependent on the fracture toughness of shale. Therefore, studying the fracture toughness of shale with different configurations and sizes is of great significance for the efficient exploitation of shale gas. Since rock materials are most prone to failure under tensile stress, mode I (tensile) fractures are the most common failure modes, and mode I inherent fracture toughness (K_{Ic}) is the focus of rock fracture mechanics research. Test methods with different configurations have been proposed to measure K_{Ic}, which can be roughly divided into two categories: artificially prefabricated notch test methods and non-prefabricated notch test methods. The former methods include the cracked chevron notched Brazilian disc (CCNBD) test (Fowell 1995; Aliha and Ayatollahi 2014), short rod (SR) test, the chevron bend (CB) test (Ouchterlony 1988), and the semi-circular bend (SCB) test (Kuruppu et al. 2014; Tutluoglu et al. 2022) recommended by International Society for Rock Mechanics (ISRM). Besides, non-standard test methods based on artificial prefabricated notches have also been widely used, such as the diametrally compressed ring (DCR) (Aliha et al. 2008), the edge cracked triangular (ECT) (Aliha et al. 2013), the edge-notched disc bend (ENDB) (Aliha and Bahmani,

2017; Bahmani and Nemati 2021), the edge-notched diametrically compressed disc (ENDC) (Aliha et al. 2021a; Bahmani et al. 2021), the single edge crack round bar bending (SECRBB) (Barr and Hasso 1986; Khan and Al-Shayea 2000; Aliha et al. 2018), the chevron notch semi-circular bend (CNSCB) (Kuruppu 1997; Mahdavi et al. 2020), and the cracked straight-through Brazilian disc (CSTBD) (Ayatollahi and Akbardoost 2014; Aliha et al. 2014; Xie et al. 2020). The latter methods include the flattened Brazilian disc (FBD) (Keles and Tutluoglu 2011) and the Brazilian disc test (BDT) (Guo et al. 1993). However, due to the large dispersion of the test data, these methods are not frequently used in fracture testing.

A growing number of studies have shown that the fracture toughness tested by different configurations of specimens varies greatly, even with the standard test methods recommended by ISRM (Aliha et al. 2017; Wei et al. 2017). For example, Aliha et al. (2017) tested the fracture toughness of rock with the SCB configuration, CB configuration, SR configuration, and CCNBD configuration recommended by ISRM, and found that the fracture toughness measured by SR specimens is twice that by CCNBD specimens. Even if the test specimens have the same configuration, the measured fracture toughness is not necessarily the same (Aliha et al. 2010; Ayatollahi and Akbardoost 2014). Aliha et al. (2010) tested the fracture toughness of CSTBD specimens with different sizes, and found that fracture toughness increases with the increase of specimen size. To explain the K_a changing with the size and configuration of the specimen, a series of fracture criteria have been proposed (Erdogan and Sih 1963; Sih 1974; Kong and Schluter, 1995). The maximum tangential stress fracture criterion is the most simple and frequently used criterion (Erdogan and Sih 1963). It is believed that the specimen will fracture when the maximum tangential stress at a certain distance from the crack tip is equal to the tensile strength of the material. The traditional maximum tangential stress (TMTS) fracture criterion ignores the influence of other stress terms on the tangential stress except for the singular terms in Williams stress expansion, and considers that the fracture of specimens with different configurations occurs under the same critical stress intensity factor. Subsequently, a modified maximum tangential stress (MMTS) fracture criterion was proposed (Aliha et al. 2012a), and the first three terms of Williams expansion were considered in determining the tangential stress near the crack tip. The MMTS criterion not only explains the size effect and configuration effect on the measurement of K_a, but also can be used to predict the K_a of the specimen (Aliha et al. 2012a, b; Ayatollahi and Akbardoost 2014; Aliha and Mousavi 2019; Bidadi et al. 2020; Sangsefidi et al. 2020). The determination of the length of the fracture process zone (FPZ) is the key to the prediction of K_a. Some studies have reported that the FPZ length is closely related to the size of the specimen (Bazant et al. 1986; Karihaloo 1999; Ayatollahi and Akbardoost 2014). Ayatollahi and Akbardoost (2014) tested the fracture toughness of CSTBD specimens with different sizes, and obtained the FPZ length by considering different terms of Williams stress expansion. It was found that the FPZ length obtained from the first three terms of Williams stress expansion is significantly larger than that obtained by the singular stress terms, and the FPZ length increases with the increase of specimen size. It indicates that the appropriate fracture criterion and the size effect of FPZ should be jointly considered in predicting the K_a. In above studies, the first three terms of Williams expansion are only considered in both the prediction of K_a and the determination of FPZ length. However, accurate results cannot be effectively obtained by this method in some cases (Wei et al. 2018). Based on the MMTS criterion, Wei et al. (2018) proposed a further maximum tangential stress (FIMTS) fracture criterion. In this criterion, more terms of Williams stress expansion should be considered to accurately describe the stress field around the crack tip.

For specimens with different sizes, the influence of boundary conditions on tangential stress at the front of the crack tip is different, while the prediction difference of the K_a of specimens with different sizes caused by TMTS, MMTS, and FIMTS criteria has never been studied. Moreover, according to the effective crack model (Nallathambi and Karihaloo 1987), the specific difference in predicting the inherent fracture toughness of the material based on the FPZ length determined by different fracture criteria is also not clear. Based on equivalent linear elastic fracture mechanics, Bazant and Planas (1997) established the failure load prediction model of specimens with different configurations from the perspective of energy release rate, namely the size effect law (SEL) model. However, the difference between the prediction results of the maximum tangential stress fracture criterion and the SEL model have not been compared in previous studies on the size effect of fracture toughness (Akbardoost et al. 2014; Akbardoost 2014; Ayatollahi and Akbardoost 2013; Sangsefidi et al. 2021). Therefore, in this paper, fracture tests of shale specimens with CSTBD configuration in different sizes were carried out. The difference between the K_a of shale specimens with different sizes was analyzed through the maximum tangential stress fracture criterion. According to test results of K_a, the TMTS, MMTS, and FIMTS criteria were used to obtain the FPZ length of specimens, and the effective crack model was used to predict the K_{Ic} of materials. To efficiently compare the effects of the TMTS, MMTS, FIMTS criteria, and the SEL model on predicting the K_a of specimens, the size effect of FPZ was also considered and three-point bending fracture tests were carried out on shale specimens with NSCB configuration.

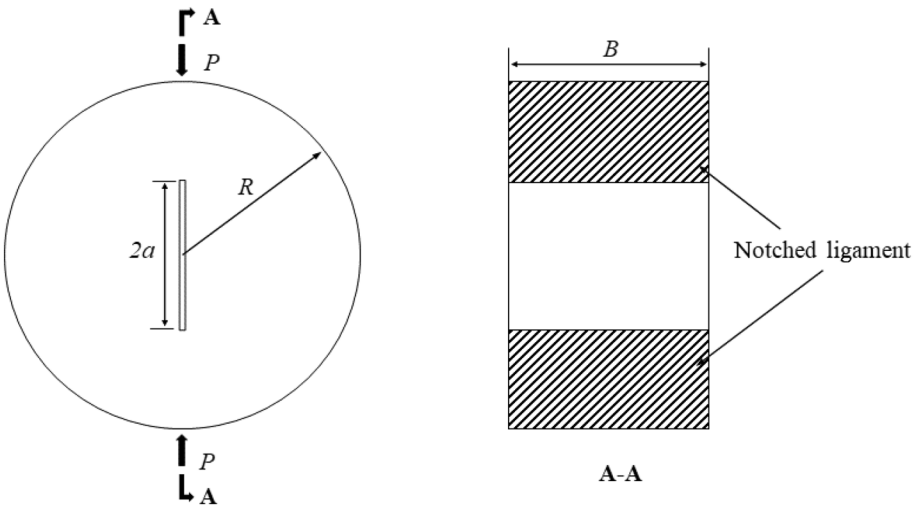

Fig. 1 Specimens with the CSTBD configuration

2 Experimental Setup

Due to the simple configuration, easy fabrication, and processing and efficient analytical solution for stress intensity factor calculation, the CSTBD configuration has been widely used in tests on rock fracture toughness. In this test, shale specimens with CSTBD configuration were selected to study the size effect of fracture toughness, as shown in Fig. 1. According to linear elastic fracture mechanics (LEFM), the mode I stress intensity factor (K_I) of CSTBD specimens can be calculated by Eqs. (1) and (2) (CAA 1981)

$$K_I = Y^* \frac{P\sqrt{\pi a}}{\pi BR}, \tag{1}$$

$$Y^* = \left[1 - \alpha + 6.24\alpha^2 - 25.44\alpha^3 + 161.6\alpha^4 - 664.96\alpha^5 + 1288.32\alpha^6 - 961.28\alpha^7\right] \Big/ \sqrt{1 - 2\alpha}, \tag{2}$$

where P is the load applied to the specimen, a *i*s half of the crack length, R is the specimen radius, B is the specimen thickness, α ($=a/R$) is the normalized crack length, and Y^* is the dimensionless stress intensity factor, which is only related to α.

Previous experimental studies have shown that the change of loading rate has a significant impact on the fracture toughness of rock (Zhang and Zhao 2013; Xu et al. 2016; Zhou et al. 2018; Ju et al. 2019). At high loading rates, the incubation time of microcracks is short, and the microcracks are mainly formed and propagated in the crystal. At low loading

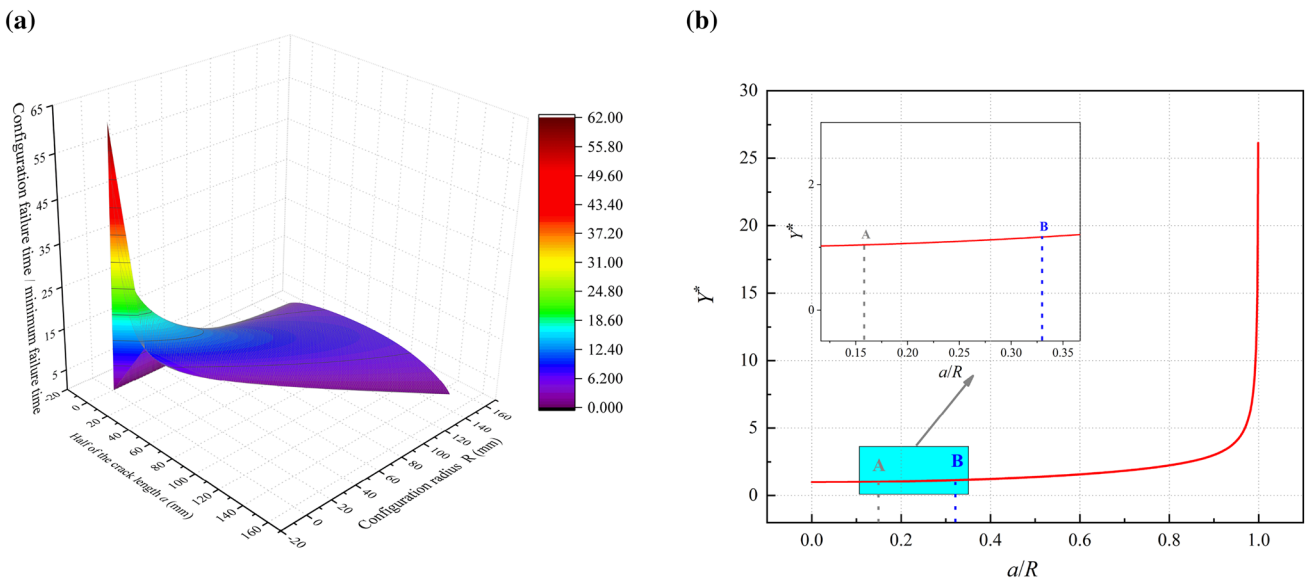

Fig. 2 **a** Failure time and **b** dimensionless stress intensity factor Y^* variation of CSTBD specimens with different sizes

Table 1 Specimen sizes for fracture tests

Specimen no	D (mm)	$2a$ (mm)	B (mm)	a/R
S-1-1	63.89	10.2	30	0.1596
S-1-2	64.12	9.9	30	0.1544
S-1-3	64.26	10	30	0.1556
S-2-1	94.12	20.4	30	0.2167
S-2-2	93.96	20.1	30	0.2139
S-2-3	94.25	19.8	30	0.2101
S-3-1	119.2	29.6	30	0.2483
S-3-2	119.15	30.2	30	0.2534
S-3-3	118.94	30	30	0.2522
S-4-1	132.22	39.8	30	0.3010
S-4-2	131.9	40	30	0.3032
S-4-3	132.11	40.2	30	0.3043

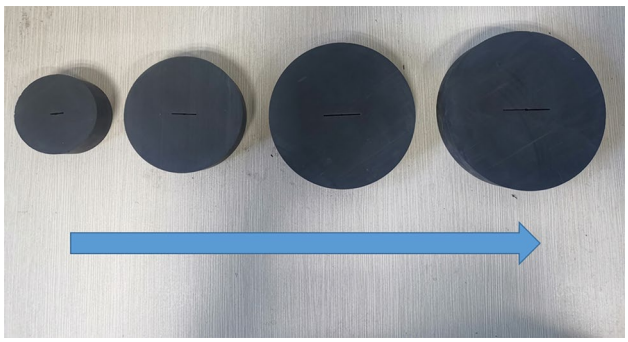

Fig. 3 The CSTBD specimens manufactured in four different sizes

Table 2 Failure loads and average K_a of CSTBD specimens with different sizes

D (mm)	P_{max} (kN)	K_a (MPa·m$^{0.5}$)
64	18.37	0.793 ± 0.047
94	21.55	0.923 ± 0.032
119	24.16	1.027 ± 0.027
132	23.51	1.078 ± 0.01

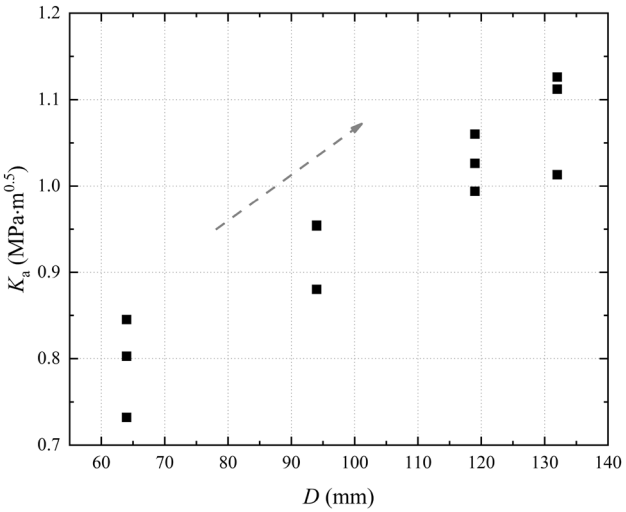

Fig. 4 The variation of K_a with specimen size

rates, microcracks have enough time to develop, the strength of crystal boundary is far lower than the resistance of crystal fracture, and the cracks prone to propagate along the crystal boundary (Liu et al. 2020). For specimens with prefabricated cracks, force-controlled loading rate, the configuration and dimensions of the specimen jointly determine the time from initial loading to complete failure. For example, when the CSTBD specimens are used under the same force-controlled loading rate, the failure time of specimens with $\alpha = 0.993$ is taken as reference, and the change of the failure time with the specimen size and the crack length can be obtained. As shown in Fig. 2a, the change of geometric configuration size can lead to the difference of failure time among specimens with different sizes by tens of times. This indicates that even at the same loading rate, the interference of rate effect may exist in measuring the size effect on fracture toughness of rock specimens. Unfortunately, the potential interference of rate effect has been rarely considered in studies. To accurately understand the effect of specimen size change on fracture toughness tests, the potential effect of loading rate should be eliminated, and the configuration size should be appropriately selected. Figure 2b shows the variation trend of dimensionless stress intensity factor Y^* with specimen configuration size derived from Eq. (2). The variation Y^* trend of CSTBD specimens is gentle ($\alpha = 0.15$–0.35), which can be regarded as a straight line. According to the K_I of CSTBD specimens in Eq. (1), when the $\sqrt{a}/R$ of specimens with different sizes are the same and the value of α is between 0.15 and 0.35, the K_I change rates of specimens with different sizes are identical under the same force-controlled loading rate, that is, based on LEFM, the specimens with different sizes can fracture at almost the same time. According to the above principles, four sizes of shale specimens were selected for the test. Table 1 shows the detailed parameters of specimen diameter D and crack length $2a$ of shale specimens.

All shale specimens were taken from the same shale rock mass to ensure high geometric integrity and uniformity. First, cores with different diameters were drilled and then cut into discs with a thickness of 30 mm. Second, a water knife was used to cut symmetrical cracks with different lengths from the center of the disc, and the notch tip was further sharpened with steel wire to form the crack tip. Figure 3 shows the processed CSTBD specimens in different sizes. Finally, the prepared specimens were tested by

the INSTRON1346 electric servo testing machine. All the specimens were directly loaded by force control through the compression plate at the loading rate of 30 N/s. The force and displacement sensors of the loader collected data automatically every 0.2 s. In addition, according to the rock tensile strength test method recommended by ISRM (1978), the tensile strength of shale was determined to be 7.927 MPa.

3 Results and Analysis

3.1 The Tested Fracture Toughness of Specimens with Different Sizes

According to the LEFM, when the external load reaches the peak load P_{max}, that is, the critical stress intensity factor is equal to the inherent fracture toughness of the material K_{Ic}, the crack begins to propagate. However, due to plastic deformation near the crack tip, the tested or apparent fracture toughness K_a is not equal to K_{Ic}, and the K_a of the CSTBD specimen can be calculated by the following equation:

$$K_I = K_a = Y^* \frac{P_{max}\sqrt{\pi a}}{\pi BR}. \tag{3}$$

Table 2 shows the failure load and average K_a of CSTBD specimens with different sizes, and Fig. 4 shows more detailed results of the K_a. It can be seen that the K_a is significantly affected by specimen size. As mentioned in Sect. 2.1, the change rate of stress intensity factor for specimens with different sizes is the same under the same force-controlled loading rate. According to the LEFM, specimens with different sizes should be broken at approximately the same time, that is, the K_a of specimens with different sizes is very close in theory. However, there is a discrepancy in test results, and larger specimens need higher loads to be fractured. As discussed in the previous studies (Smith et al. 2010; Ayatollahi and Akbardoost 2014; Wei et al. 2018), such experimental results are understandable when the stress field near the crack tip is determined by considering other terms other than the singular term in Williams stress expansion. Because shale is a kind of quasi-brittle material, there is an inevitable FPZ near the crack tip, which will enlarge the influence of other stress terms on the fracture behavior of specimens. The results of this experiment clearly show the limitations of LEFM and the influence of FPZ on the failure load of specimens.

3.2 Comparison of Stress Field Distribution Determined by Different Fracture Criteria

To comprehensively explain the size effect of K_a observed in the test, the maximum tangential stress fracture criterion

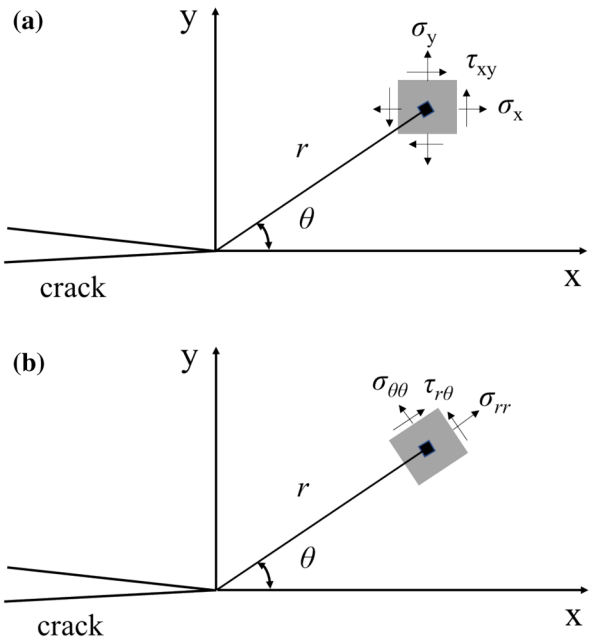

Fig. 5 Stress components near the crack tip in **a** rectangular coordinate system; **b** polar coordinate system

is used to analyze the test results in detail. According to the well-known Williams stress expansion (Williams 1957), the stress around the crack tip of the plate with cracks under the action of the load in the plane can be described by Eq. (4) in line with the coordinate system in Fig. 5

$$\begin{Bmatrix}\sigma_x\\ \sigma_y\\ \sigma_z\end{Bmatrix} = \sum_{n=1}^{\infty}\frac{n}{2}A_n r^{\left(\frac{n}{2}-1\right)} \begin{Bmatrix}\left(2+\frac{n}{2}+(-1)^n\right)\cos\left(\frac{n}{2}-1\right)\theta-\left(\frac{n}{2}-1\right)\cos\left(\frac{n}{2}-3\right)\theta\\ \left(2+\frac{n}{2}-(-1)^n\right)\cos\left(\frac{n}{2}-1\right)\theta+\left(\frac{n}{2}-1\right)\cos\left(\frac{n}{2}-3\right)\theta\\ \left(\frac{n}{2}-1\right)\sin\left(\frac{n}{2}-3\right)\theta-\left(\frac{n}{2}+(-1)^n\right)\sin\left(\frac{n}{2}-1\right)\theta\end{Bmatrix} - \sum_{n=1}^{\infty}\frac{n}{2}B_n r^{\left(\frac{n}{2}-1\right)} \begin{Bmatrix}\left(2+\frac{n}{2}-(-1)^n\right)\sin\left(\frac{n}{2}-1\right)\theta-\left(\frac{n}{2}-1\right)\sin\left(\frac{n}{2}-3\right)\theta\\ \left(2-\frac{n}{2}+(-1)^n\right)\sin\left(\frac{n}{2}-1\right)\theta+\left(\frac{n}{2}-1\right)\sin\left(\frac{n}{2}-3\right)\theta\\ -\left(\frac{n}{2}-1\right)\cos\left(\frac{n}{2}-3\right)\theta+\left(\frac{n}{2}-(-1)^n\right)\cos\left(\frac{n}{2}-1\right)\theta\end{Bmatrix}, \tag{4}$$

where r and θ are polar coordinates, n is the serial number of the term in the infinite series, and the coefficients A_n and B_n depend on the configuration and geometry of the specimen and the applied load.

The maximum tangential stress fracture criterion proposed that when the maximum tangential stress at a certain distance r_c from the crack tip reaches the critical value f_t, the specimen will fracture. In this study, r_c and f_t are considered

to be the FPZ length and the tensile strength of the material. For mode I fracture, the maximum tangential stress appears at the front of the crack tip, that is, $\theta=0$. By substituting $\theta=0$ into Eq. (4), the tangential stress at the location r away from the crack tip is obtained

$$\begin{aligned}\sigma_{\theta\theta}=\sigma_y|_{\theta=0}&=\sum_{n=1}^{\infty}\frac{n}{2}A_n r^{\left(\frac{n}{2}-1\right)}(1-(-1)^n)\\&=A_1 r^{-\frac{1}{2}}+3A_3 r^{\frac{1}{2}}+5A_5 r^{\frac{3}{2}}+7A_7 r^{\frac{5}{2}}\\&\quad+9A_9 r^{\frac{7}{2}}+11A_{11} r^{\frac{9}{2}}+13A_{13} r^{\frac{11}{2}}+\cdots,\end{aligned}\tag{5}$$

where the first term is called singular term, which is also the term of well-known stress intensity factor K_I. Therefore, the coefficient A_1 can be expressed by K_I

$$A_1=\frac{K_I}{\sqrt{2\pi}}.\tag{6}$$

As expressed in Eq. (5), when r is small and infinitely close to 0, two extremes are caused, that is, the first term of Williams stress expansion becomes very large, while other stress terms tend to 0. Compared with the first term, the influence of other stress terms can be completely ignored, and the stress field near the crack tip can be described by the stress intensity factor alone. The TMTS criterion only considers the effect of singular terms on the fracture behavior of the specimen and infers that the K_a obtained in fracture tests is the same. Therefore, the K_a is only related to the properties of the material. However, this is very different from the actual fracture test results. Many studies have shown that the K_a is related to the configuration and size of the specimen (Aliha et al. 2010, 2017; Ayatollahi and Akbardoost 2014). Similar results are also obtained in this test, and the K_a is significantly affected by specimen size.

For quasi-brittle materials (such as rocks, concrete and hard clay), the FPZ length is relatively large, and the influence of other stress terms cannot be directly ignored. If the singular term is only considered to describe the stress field

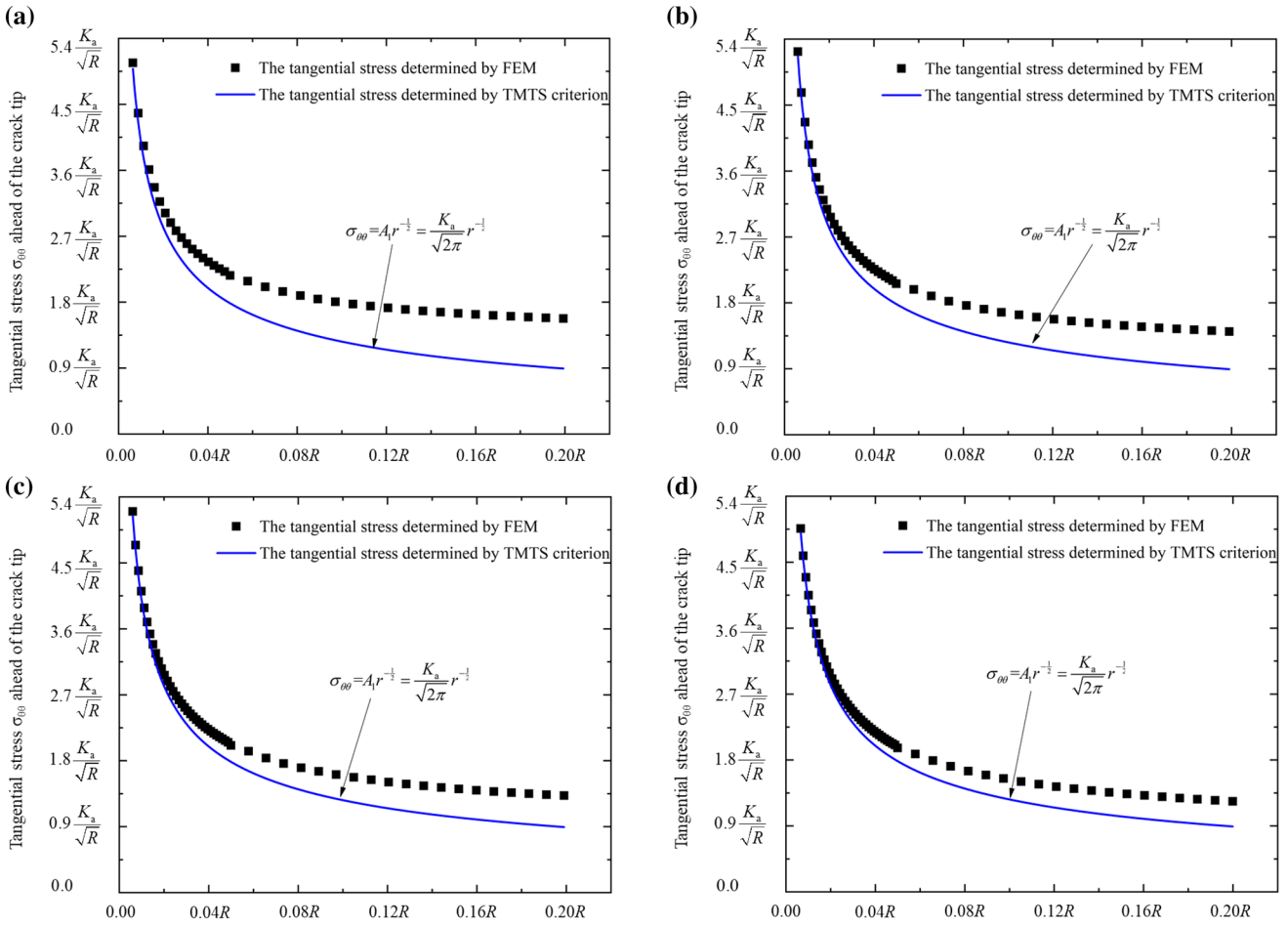

Fig. 6 Comparison of tangential stress determined by FEM and TMTS criteria for CSTBD specimens with different sizes: **a** 64 mm; **b** 94 mm; **c** 119 mm; **d** 132 mm

at a certain distance from the crack tip, the mode I fracture behavior of rock specimens cannot be accurately evaluated. To this end, the tangential stress at the crack tip front of the specimen was extracted by the ABAQUS software. Due to the symmetry of loading conditions and specimen configuration, only a quarter of CSTBD specimens is selected for analysis, and a quarter node element is used at the crack tip regions to simulate the stress singularity near the crack tip.

The dimensionless stress intensity factor Y^* of the CSTBD specimens with normalized crack length of 0.156, 0.213, 0.252, and 0.303 are 1.037, 1.067, 1.094, and 1.137, respectively. For simplicity, the specimen size and thickness are treated as unknown quantities. According to Eq. (3) in Sect. 3.1, the failure loads of CSTBD specimen with diameters of 64 mm, 94 mm, 119 mm, and 132 mm are $4.324K_aB\sqrt{R}$, $3.601K_aB\sqrt{R}$, $3.227K_aB\sqrt{R}$, and $2.832K_aB\sqrt{R}$, respectively. After applying appropriate boundary conditions and fracture loads in the ABAQUS software, the tangential stress at the crack tip front can be extracted by a simple numerical calculation.

Figure 6 shows the tangential stress distribution at the crack tip front of specimens with different sizes. For comparison, the tangential stress field described by the TMTS criterion (the singular term) is also drawn. In the region near the crack tip, the tangential stress at the front of the crack tip determined by FEM and TMTS criteria is almost the same. However, as the observation point is far away from the crack tip, the gap between them becomes larger and larger. It further shows that the tangential stress of region far away from the crack tip cannot be accurately described through the simple consideration of singular terms. At the same time, for CSTBD specimens, the tangential stress at the crack tip described by the TMTS criterion is always lower than that extracted by FEM. This explains the phenomenon that the K_a determined by some configurations is always lower than the K_{Ic} of the materials.

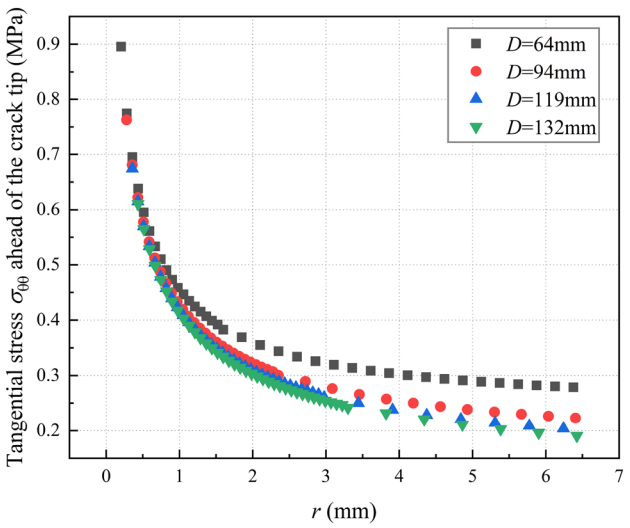

Fig. 7 Comparison of tangential stress by FEM at crack tip for CSTBD specimens with different sizes

To further compare the influence of higher order stress terms on the tangential stress near the crack tip, the tangential stress extracted by the FEM at the crack tip front of CSTBD specimens with different sizes is plotted together, as shown in Fig. 7. It should be noted that the stress intensity factor of specimens is set as 1 MPa·m$^{0.5}$ in Fig. 7. There are obvious differences in the tangential stress field of specimens with different sizes. The results show that when the TMTS criterion is used to describe the tangential stress field at the front of crack tip, a large error can be caused in the analysis of material fracture, especially for plastic materials. Besides, the TMTS criterion cannot explain the size effect of fracture toughness in this experiment.

The TMTS criterion is merely suitable for ideal brittle materials, while most of the materials in practical engineering are quasi-brittle materials or plastic materials, and large deviation can be caused by TMTS criterion in the actual situation. Considering the influence of the first three terms of Williams stress expansion on the fracture behavior of specimen, Aliha et al. (2012a) proposed the modified maximum tangential stress (MMTS) fracture criterion based on the TMTS criterion. The MMTS criterion can explain the inconsistency of fracture toughness obtained from specimens with different configurations or sizes. As shown in Fig. 8, the tangential stress distribution determined by MMTS criterion is much closer to that determined by FEM, followed by that determined by TMTS criterion. It shows that the MMTS criterion can more accurately describe the fracture behavior of specimens than the TMTS criterion.

Although the MMTS criterion modifies the description of the tangential stress field by the TMTS criterion to a certain extent, there are still non-negligible errors for small-size specimens, as shown in Fig. 8a, b. Based on the MMTS criterion, Wei et al. (2018) proposed a further maximum tangential stress (FIMTS) fracture criterion. It is believed that more terms of Williams expansion should be selected to determine the tangential stress field. Using the Levenberg–Marquardt optimization algorithm, the tangential stress of four specimens with different sizes determined by FEM is fitted by nonlinear polynomial by Eq. (5), as shown in Fig. 9. The specific fitting expression is also illustrated in this figure. For specimens with four sizes in this study, the tangential stress can be accurately described by selecting the first seven terms of the Williams stress expansion, and the coefficients of determination can reach 0.999. Therefore, the FIMTS criterion considering the first seven terms of the Williams stress expansion is adopted for subsequent analysis.

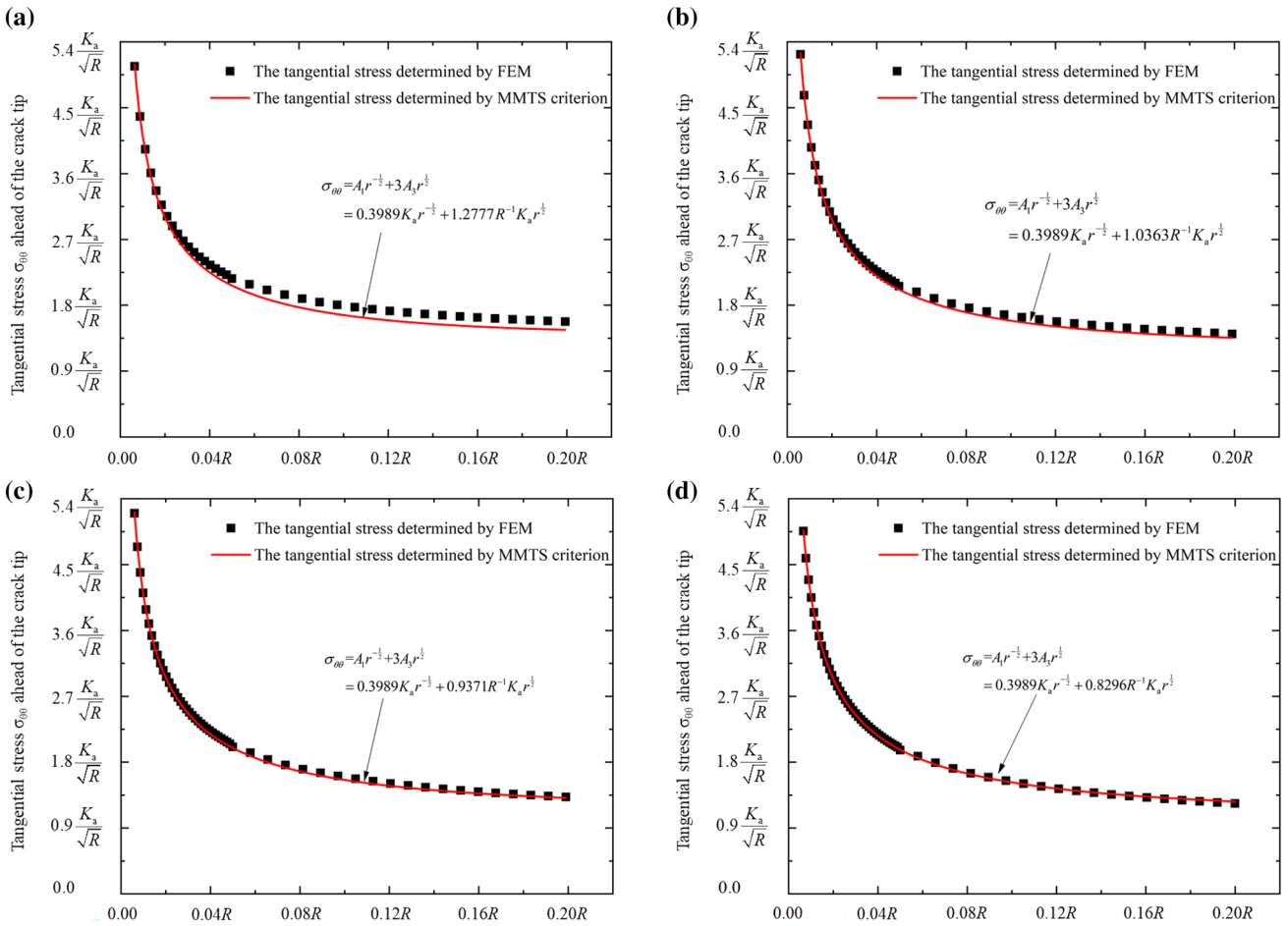

Fig. 8 Comparison of tangential stress determined by FEM and MMTS criteria for CSTBD specimens with different size: **a** 64 mm; **b** 94 mm; **c** 119 mm; **d** 132 mm

4 Prediction of Fracture Toughness

4.1 Prediction of K_{Ic} of Shale Specimens

According to the maximum tangential stress fracture criterion, when the maximum tangential stress on the boundary of the FPZ is equal to the tensile strength of the material, the specimen will fracture. Therefore, the conditions for judging specimen fracture by the TMTS criterion can be expressed by Eq. (7)

$$\frac{K_a}{\sqrt{2\pi}} r_c^{-\frac{1}{2}} = f_t. \tag{7}$$

Similarly, the valid conditions for MMTS and FIMTS criteria for judging specimen fracture can be expressed by Eqs. (8) and (9), respectively

$$\frac{K_a}{\sqrt{2\pi}} r_c^{-\frac{1}{2}} + 3A_{3c} r_c^{\frac{1}{2}} = f_t, \tag{8}$$

$$\begin{aligned} &\frac{K_a}{\sqrt{2\pi}} r_c^{-\frac{1}{2}} + 3A_{3c} r_c^{\frac{1}{2}} + 5A_{5c} r_c^{\frac{3}{2}} + 7A_{7c} r_c^{\frac{5}{2}} \\ &+ 9A_{9c} r_c^{\frac{7}{2}} + 11A_{11c} r_c^{\frac{9}{2}} + 13A_{13c} r_c^{\frac{11}{2}} = f_t, \end{aligned} \tag{9}$$

where A_{ic} $(i = 1, 2, 3\ldots)$ is the critical value of the coefficient of the Williams expansion.

For the Brazilian disc specimen, Aliha (2014) and Aliha et al. (2021b) found that the tensile strength of the tested specimen depends on the thickness/diameter ratio of the specimen. Small tensile strength will make the fracture process zone length determined based on the maximum tangential stress fracture criterion larger. This study used the method recommended by ISRM for determining tensile strength of rock materials to obtain reliable tensile strength,

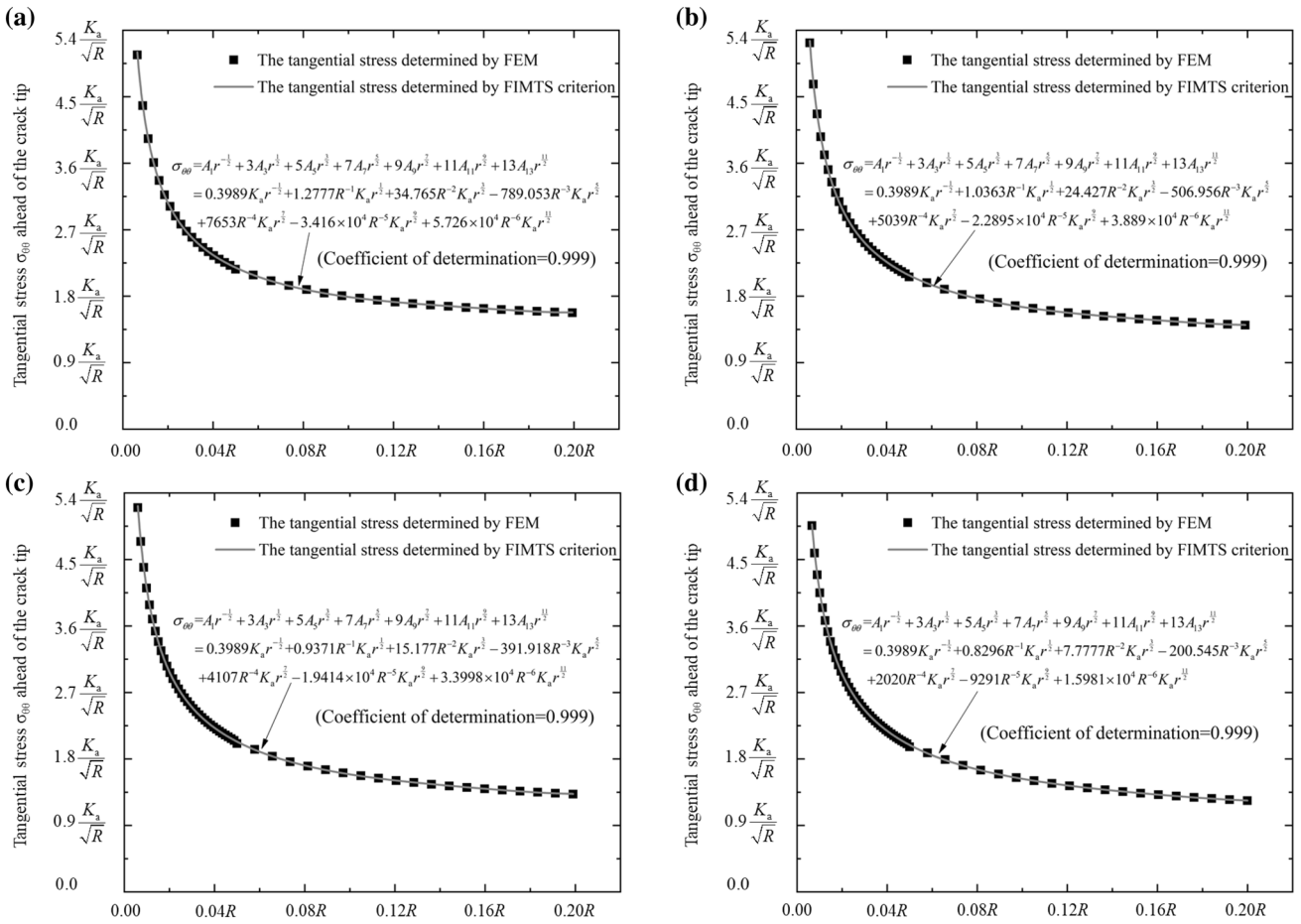

Fig. 9 The coefficients of Williams expansion obtained by fitting the FEM-determined tangential stresses for CSTBD specimens with different sizes: **a** 64 mm; **b** 94 mm; **c** 119 mm; **d** 132 mm

Table 3 The FPZ lengths determined by different fracture criteria

D(mm)	r_c (mm)		
	TMTS criterion	MMTS criterion	FIMTS criterion
64	1.592	2.4819	3.217
94	2.157	2.9059	3.232
119	2.671	3.4473	3.644
132	2.943	3.5709	3.7544

and the tensile strength value has been given in Sect. 2. According to the K_a obtained by fracture tests of CSTBD specimens in Sect. 3.1, the FPZ lengths were obtained by different fracture criteria, as listed in Table 3. It can be found that the FPZ lengths obtained by the FIMTS criterion are the largest, while the FPZ lengths obtained by the TMTS criterion considering only the singular term are the smallest. This is mainly because the tangential stress determined by the TMTS criterion is obviously lower than that determined by the FIMTS criterion. It is worth noting that for small-size

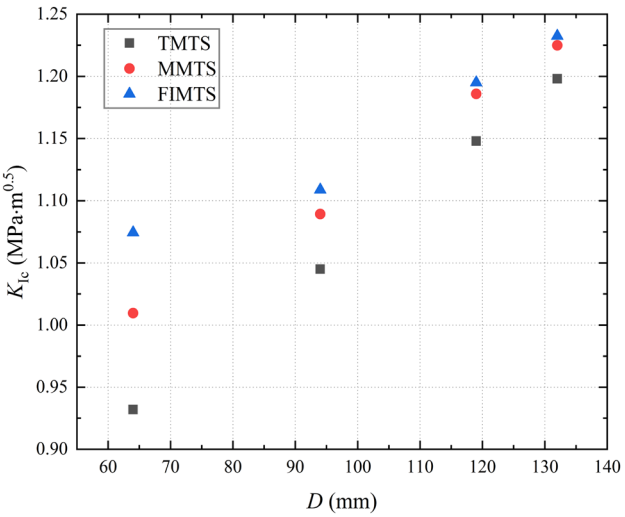

Fig. 10 The K_{Ic} of shale obtained by the effective crack model

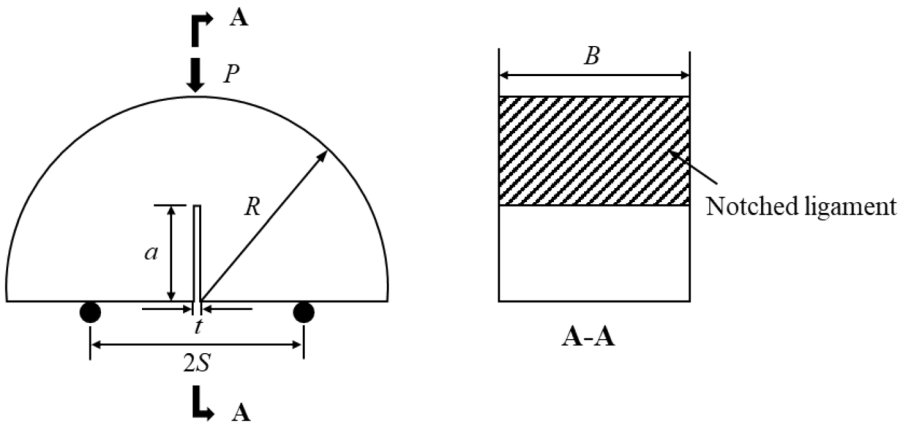

Fig. 11 The loading diagram of NSCB specimens

specimens, the difference between the FPZ lengths determined by the FIMTS criterion and the TMTS criterion is the largest. With the increase of the specimen size, the difference between the FPZ lengths determined by the three fracture criteria gradually decreases, which indicates that the FPZ lengths of large-size specimens are less affected by the selection of fracture criteria. There is still a certain gap between the FPZ lengths obtained by the MMTS criterion and that obtained by the FIMTS criterion, especially for small-size specimens.

According to the effective crack model, the effective crack length a_{ec} of the specimen can be calculated by Eq. (10)

$$a_{ec} = a + r_c. \tag{10}$$

For CSTBD specimens, the mode I fracture toughness is calculated by Eq. (3), and the ratio of K_a to K_{Ic} is obtained as follows:

$$\frac{K_a}{K_{Ic}} = \sqrt{\frac{a_{ec}}{a}} \frac{Y^*(\alpha_{ec})}{Y^*(\alpha)}, \tag{11}$$

where α_{ec} ($=a_{ec}/R$) is normalized effective crack length. The previously determined FPZ lengths and K_a of shale specimens are substituted into Eq. (11). Figure 10 shows the calculation results of K_{Ic}. Regardless of the selection of criterion in determining the FPZ length, the difference of K_{Ic} of each size specimen after the correction of the effective crack model is smaller than that between the K_a. Since the K_{Ic} of materials is only related to the properties of materials, from this point of view, the fracture toughness obtained by the effective crack model is more reliable. At the same time, the fluctuation of K_{Ic} obtained from the FPZ lengths determined by the FIMTS criterion is the smallest, followed by the MMTS criterion and the TMTS criterion, which further shows that the FIMTS criterion is most suitable for describing the fracture behavior of materials. When the effective crack model is used to predict the K_{Ic} of materials, the FPZ lengths determined by the FIMTS criterion are preferred. In addition, with the increase of specimen size, the difference between the K_{Ic} determined by the three fracture criteria decreases gradually. When the specimen size is 132 mm, the difference between the K_{Ic} determined by the TMTS criterion and the FIMTS criterion is only 0.0345 MPa·m$^{1/2}$. As mentioned in Sect. 3, the tangential stress determined by either fracture criterion is very close to that extracted by FEM for large-size specimens. It shows that the region controlled by the singular term increases with the increase of specimen size. Therefore, when the specimen size increases to a certain extent, the FPZ length is very small or can be ignored compared with the region controlled by the singular term. Besides, the TMTS criterion can be directly used to describe the fracture behavior of materials. This is the essential reason why the larger the specimen size is, the larger the K_a is. When the specimen size tends to infinity, the K_a is the K_{Ic} of the material.

4.2 Prediction of K_a of NSCB Specimens

To compare the prediction effect of the TMTS criterion, MMTS criterion, FIMTS criterion, and SEL model on the K_a of specimens, a three-point bending fracture test on NSCB specimens was carried out. Figure 11 shows the loading diagram of NSCB specimens.

According to the fracture toughness test method of NSCB specimens recommended by ISRM (Kuruppu et al. 2014), the parameters of specimens are as follows: $a=20$ mm, $R=40$ mm, and $B=30$ mm. The support frame span $2S=50$ mm. The fracture test was carried out on a biomechanics testing machine with a loading rate of 0.1 mm/min. The K_a of the NSCB specimen is calculated by Eqs. (12) and (13) (Aliha et al. 2017)

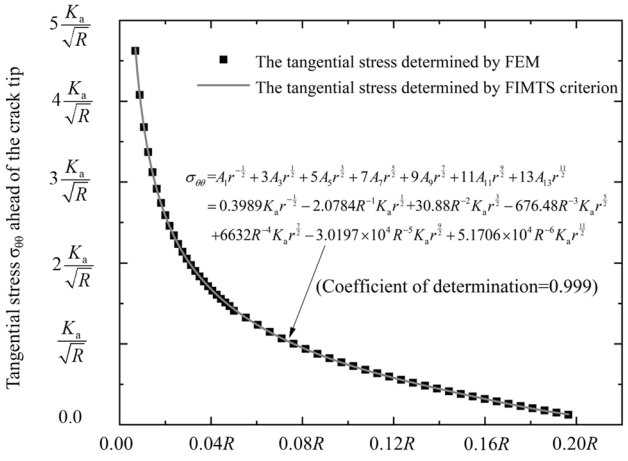

Fig. 12 The coefficients of Williams expansion obtained by fitting the FEM-determined tangential stresses for NSCB specimens

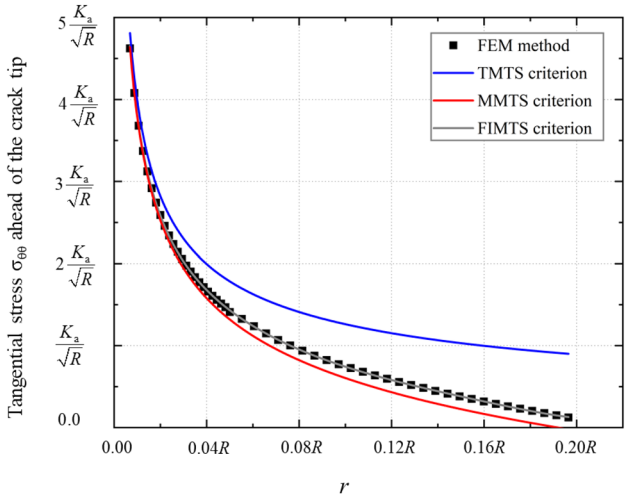

Fig. 13 Tangential stress distribution near the crack tip determined by different fracture criteria for NSCB specimens

$$K_a = Y^* \frac{P_{max}\sqrt{\pi a}}{2RB}, \tag{12}$$

$$Y^* = -1.297 + 9.516(S/R) - (0.47 + 16.457(S/R))\,\alpha + (1.071 + 34.401(S/R))\alpha^2. \tag{13}$$

After three repeated tests, the average failure load of the specimen is 3070 N, and the K_a of shale specimens with the NSCB configuration is 1.5761 MPa·m$^{1/2}$.

4.2.1 Prediction Results of the Maximum Tangential Stress Fracture Criterion

In contrast to the solution process of FPZ length in Sect. 4.1, the FPZ length is taken as a known quantity and substituted into Eqs. (7), (8) and (9) in the prediction of K_a. Therefore, the determination of FPZ length plays an important role in predicting the results. The TMTS, MMTS, and FIMTS criteria based on the maximum tangential stress fracture criterion are introduced in Sect. 3.2 and will not be repeated here.

Before applying the maximum tangential stress fracture criterion, the distribution of tangential stress at the front of crack tip should be determined first, that is, the values of the coefficients in Williams stress expansion should be obtained. The FEM was also used in the calculation of Williams expansion coefficient of NSCB configuration, which is the same as that of CSTBD specimens before. The tangential stress was extracted after the fracture load of $0.3246K_aBR^{1/2}$ and appropriate boundary conditions were applied in the finite-element model of NSCB configuration. Figure 12 shows the fitting results of the first seven Williams stress expansion terms to the tangential stress with the determination coefficients reaching 0.999.

According to the fitting results, the relationship between K_a and the FPZ length based on the TMTS criterion, MMTS criterion, and FIMTS criterion is expressed by Eqs. (14), (15) and (16), respectively

$$K_a = f_t\sqrt{2\pi r_c}, \tag{14}$$

$$f_t = 0.3989K_a r_c^{-\frac{1}{2}} - 0.05196K_a r_c^{\frac{1}{2}}, \tag{15}$$

$$f_t = 0.3989K_a r_c^{-\frac{1}{2}} - 0.05196K_a r_c^{\frac{1}{2}} + 0.0193K_a r_c^{\frac{3}{2}} - 0.01057K_a r_c^{\frac{5}{2}} + 0.00259K_a r_c^{\frac{7}{2}} - 0.000295K_a r_c^{\frac{9}{2}} + 0.0000126K_a r_c^{\frac{11}{2}}. \tag{16}$$

Table 4 The K_a of NSCB specimens predicted by three fracture criteria

r_c (mm)		Experimental result K_a (MPa·m$^{1/2}$)	The predicted result K_a (MPa·m$^{1/2}$)		
			TMTS criterion	MMTS criterion	FIMTS criterion
TMTS criterion	2.157	1.5761	0.9228	1.283	1.172
MMTS criterion	2.9059		1.07112	1.7237	1.5118
FIMTS criterion	3.232		1.1296	1.9512	1.677

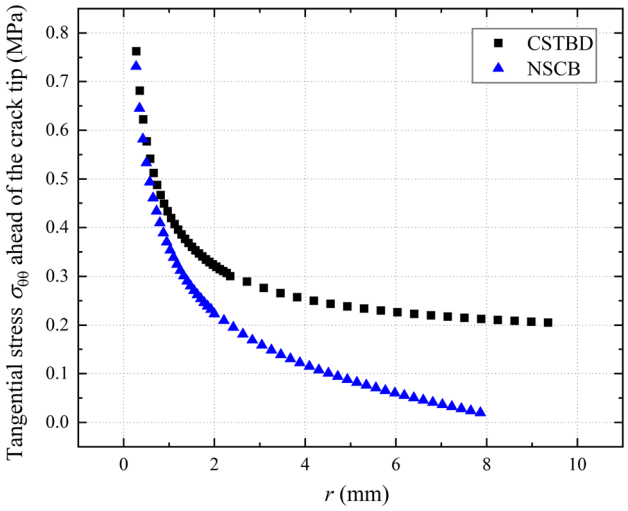

Fig. 14 Tangential stress near the crack tip of CSTBD and NSCB specimens under the same stress intensity factor

To predict the K_a of the specimen, the FPZ length of the specimen with NSCB configuration should be obtained first. In this study, due to the size effect of FPZ, it is considered that the FPZ length of the NSCB specimen with a diameter of 80 mm is the same as that of the CSTBD specimen with a diameter of 94 mm (since the diameter of the NSCB specimen is 80 mm, which is closest to that of the CSTBD specimen with a diameter of 94 mm). Table 4 lists the K_a of NSCB specimens predicted by TMTS, MMTS, and FIMTS criteria by Eqs. (14), (15) and (16). It can be found that the K_a predicted by the FPZ length using the MMTS criterion is closer to the tested fracture toughness, followed by the K_a predicted by the FPZ length using the FIMTS criterion. However, the research of Ayatollahi and Akbardoost (2014) shows that the prediction effect of K_a is the best when the fracture criterion for determining the FPZ length is consistent with the prediction criterion. Considering that the K_a predicted by the two criteria is very close in this study, it may be that the placement error of the specimen during the fracture test affects the test results. Ideally, the experimental results should be consistent with those of Ayatollahi and Akbardoost (2014).

Comparing the prediction results of each fracture criterion, it can be found that the change of FPZ length has the greatest influence on the K_a predicted by the MMTS criterion. For any FPZ length, the K_a predicted by the MMTS criterion is the largest among the three fracture criteria. Figure 13 shows the tangential stress distribution determined by different fracture criteria under the condition of equal stress intensity factors. In the region of 1.6–3.2 mm away from the crack tip, the tangential stress determined by the MMTS criterion changes most significantly. As a result, the change of FPZ length can easily affect the prediction result using the MMTS criterion. The tangential stress determined by the MMTS fracture criterion is less than that determined by the other two fracture criteria. Under the condition of the same FPZ length, if the tangential stress of the three fracture criteria on the boundary of FPZ is to reach the same value, then the singular term of the MMTS criterion must be larger than that of the other two fracture criteria; thus, the K_a predicted by the MMTS criterion is higher than that predicted by the TMTS and FIMTS criteria.

Reviewing the fracture test results of CSTBD specimens in Sect. 3.1, the fracture toughness tested by NSCB specimens is much larger than that tested by CSTBD specimens. Figure 14 shows the tangential stress distribution near the crack tip of NSCB specimens and CSTBD specimens with a stress intensity factor of 1 MPa·m$^{1/2}$. It is found that the tangential stress of CSTBD specimens and NSCB specimens in the region close to the crack tip is almost the same. However, as the distance from the crack tip increases, the stress difference between the two configurations also increases, mainly because the higher order term of Williams expansion affects the far-field stress distribution. At the same distance from the crack tip, the tangential stress of CSTBD specimens is always greater than that of NSCB specimens, which indicates that CSTBD specimens are more prone to failure than NSCB specimens with the same material under the same stress intensity factor. As a result, the fracture toughness tested by CSTBD specimens is far less than that of NSCB specimens. It is expected that this phenomenon will be more significant in materials with low tensile strength or plastic materials.

4.2.2 Prediction Results of SEL Model

The above-mentioned maximum tangential stress fracture criteria analyze the fracture behavior of rock materials by different terms of the Williams stress expansion, while the SEL model supports that the crack will propagate subcritical before material fracture without considering the change of stress near the crack tip. In addition, the maximum tangential stress fracture criterion is based on the relationship between the stress and the strength of the material to judge the fracture of the specimen, while the fracture evaluation condition of the SEL model is whether the strain energy released per unit length of crack propagation reaches the fracture energy of the material. In other words, the theoretical basis proposed by the SEL model and the maximum tangential stress fracture criterion is quite different, but both of them believe that the FPZ near the crack tip can affect the strength of the specimen. It can also be understood that the most essential reason for the difference in the K_a determined by different configurations is the existence of the FPZ. According to

LEFM, when a structure is subjected to nominal stress σ_N, the expression of stress intensity factor K_I is as follows:

$$K_I = \sigma_N \sqrt{L} k(\alpha), \tag{17}$$

where L and $k(\alpha)$ denote the characteristic length and dimensionless functions. Therefore, the energy release rate $G(\alpha)$ per unit length of crack propagation can be written as

$$G(\alpha) = \frac{K_I^2}{E} = \frac{\sigma_N^2 L}{E} g(\alpha). \tag{18}$$

Here, $g(\alpha) = k(\alpha)^2$ represents the dimensionless energy release rate, and E represents the elastic modulus of the material. Based on equivalent LEFM, the maximum loads for specimens with various sizes may be assumed to occur when the tip of the equivalent elastic crack is at a certain distance c ahead of the tip of the initial crack. Therefore, the length of c should also be considered in the effective crack length in the calculation of the energy release rate. When the specimen size tends to infinity, the corresponding value of c in the SEL model is denoted as c_f, and the following equation can be established:

$$G(\alpha_0 + c_f/L) = \frac{\sigma_{Nu}^2 L}{E} g(\alpha_0 + c_f/L) = G_f, \tag{19}$$

where G_f is the fracture energy and belongs to the material constant; σ_{Nu} is the nominal failure stress of the specimen and α_0 is the ratio of the length of the prefabricated crack to the characteristic length of the specimen. By approximating $g(\alpha_0 + c_f/L)$ with its Taylor series expansion at α_0 and retaining only up to the linear term of the expansion, Eq. (20) can be obtained

$$\sigma_{Nu} = \sqrt{\frac{E * G_f}{L g(\alpha_0) + c_f g'(\alpha_0)}}. \tag{20}$$

Equation (20) is replaced with the following simple variables as follows:

$$X = L, \quad Y = \sigma_N^{-2}, \tag{21}$$

$$A = \frac{g(\alpha_0)}{E * G_f}, \quad C = \frac{c_f g'(\alpha_0)}{E * G_f}. \tag{22}$$

Then, the relationship between failure stress and specimen size established by the traditional SEL model is as follows:

$$Y = AX + C, \tag{23}$$

where A and C are constants related to E, G_f, and c_f. The values of A and C can be obtained by the linear fitting method with sufficient test data. According to the relationship between failure stress and specimen size, the K_a of specimens in any size can be predicted. The premise of the application of the traditional SEL model is that the ratio of the length of crack to the characteristic length of the specimen with different sizes is equal to a constant. However, it is difficult to ensure the extreme similarity of the specimen geometry in the process of rock specimen manufacturing. Besides, the size of the target configuration that needs to be predicted is also varied, which seriously limits the application of the SEL model. Therefore, the improved SEL model is proposed, in which the configuration parameters of the specimen are put in the independent variables, and the influence of the specimen configuration factors before building the model is considered. Several variables are converted as follows:

$$X = \frac{g(\alpha_0)}{g'(\alpha_0)} L, \quad Y = \frac{1}{g'(\alpha_0)\sigma_{Nu}^2}, \tag{24}$$

Table 5 Basic parameters of CSTBD specimens for prediction

D (mm)	Parameters				
	σ_{Nu}	$g(\alpha)$	$g'(\alpha)$	X	Y
64	19.135	0.1373	2.5683	4.3936	0.00701
94	15.283	0.1701	2.2055	7.9947	0.00944
119	13.535	0.1873	1.9482	11.14435	0.01063
132	11.874	0.2035	1.6322	13.432	0.01158

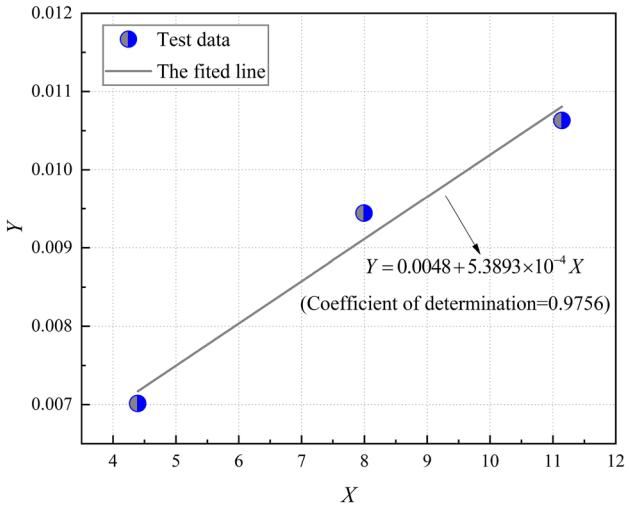

Fig. 15 Fitting results based on the test data of CSTBD specimens with diameters of 64 mm, 94 mm, and 119 mm

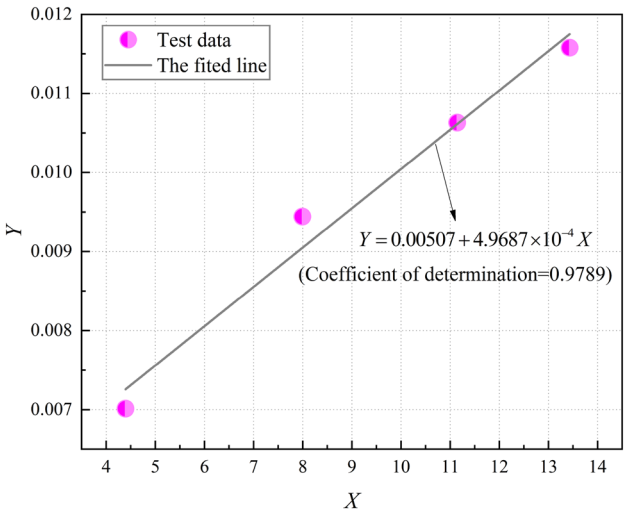

Fig. 16 Fitting results based on the test data of CSTBD specimens of all sizes

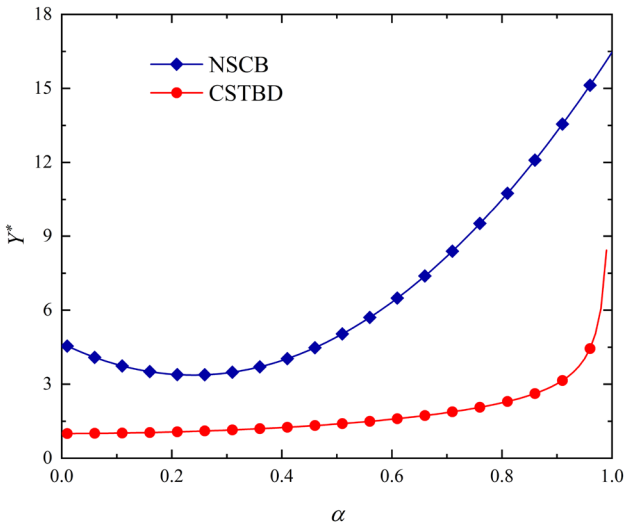

Fig. 17 The dimensionless stress intensity factor of the CSTBD and NSCB specimens at various crack lengths

$$A' = \frac{1}{E * G_f}, \quad C' = \frac{c_f}{E * G_f}. \tag{25}$$

Therefore, Eq. (20) can be written as follows:

$$Y = A'X + C'. \tag{26}$$

The application of Eq. (26) has no restrictions on the geometry and size of the test specimen and the predicted specimen, but needs to solve the dimensionless stress intensity factor expression of the test specimen and the predicted specimen in advance.

The expression of stress intensity factor of CSTBD specimens has been given in Sect. 2.1, so it will not be deduced here. According to Eq. (17), some parameters of CSTBD specimens are described as follows:

$$\sigma_N = \frac{P}{BR}, \tag{27}$$

$$k(\alpha) = \sqrt{\frac{a}{R}\frac{1}{\pi}} Y^*. \tag{28}$$

According to Eqs. (24) and (25), the basic parameters for prediction are obtained, as listed in Table 5. The K_a of CSTBD specimens with diameters of 64 mm, 94 mm and 119 mm were used as test data to predict the K_a of specimens with diameters of 132 mm. According to the data in Table 5 and the relationship between Y and X in Eq. 26, the linear fitting of X and Y was carried out, as shown in Fig. 15. It is found that there is a good linear relationship between Y and X, which indicates that the relationship between failure loads of CSTBD specimens with different sizes can be well described by the SEL model. According to the fitting results, the relationship between Y and X can be expressed as follows:

$$Y = 0.0048 + 5.3893 \times 10^{-4} X. \tag{29}$$

For the CSTBD specimen with a diameter of 132 mm, the X value is 13.432, the predicted value of Y is 0.01204 by Eq. (29), while the Y value obtained by fracture test is 0.01158, the difference between the two is only 0.00046, and the prediction error is only 3.97%. It further shows that the SEL model can be used to predict the failure load of CSTBD specimens. To accurately describe the relationship between failure load and specimen size, the fracture toughness of CSTBD specimens with diameters of 132 mm is also used for fitting. As shown in Fig. 16, there is still a linear relationship between Y and X obtained from the test data of four-size specimens. The relationship between Y and X can be expressed by Eq. (30)

$$Y = 0.00507 + 4.9687 \times 10^{-4} X. \tag{30}$$

The values of c_f and G_f can be obtained from the relationship between the intercept of the fitting line and the slope of the line in Eq. (25). For the NSCB specimens, the value of X is 5.876 by Eqs. (12) and (17), and the value of Y is 0.00798 by substituting it into Eq. (30). According to the definition of Y in Eq. (24), the predicted failure load of NSCB specimen after conversion is 1677.8 N, which is obviously different from that of the test, and the difference is about twice. It is thought that the value of c_f in the SEL model can be understood as a reference length. The foundation of the SEL model is that the fracture energy of the material is

equal to the energy release rate of the specimen calculated by taking the prefabricated crack length plus the reference length as the final crack length. Since the fracture energy G_f of the material is fixed, the reference length c_f determines the prediction result of apparent fracture toughness from Eq. 19. In the actual test process, due to the influence of various factors, the c_f fitted by the test data will inevitably deviate from its theoretical value. Because the dimensionless energy release rate $g(\alpha)$ mainly depends on the dimensionless stress intensity factor Y^*, and the Y^* of predicted configuration not change greatly with α, the change of c_f has little impact on the prediction results, even difficult to observe it. On the contrary, the prediction results will be far from the test results. For example, as shown in Fig. 17, the $Y^*$of CSTBD configuration changes gently with α from 0.15 to 0.35, while the Y^* of NSCB configuration changes greatly with α greater than 0.5. In previous test results, it has been found that the change of fracture toughness of CSTBD specimens with different sizes conforms to SEL model, while the tested fracture toughness of NSCB specimens is quite different from the predicted value by SEL model base on the test data of CSTBD specimens. This shows that the application of SEL model needs to strictly ensure the accuracy of each set of test data, especially for the configuration in which Y^* changes greatly with α.

The K_a prediction process in the SEL model is obviously different from that in the maximum tangential stress fracture criterion. In principle, the maximum tangential stress fracture criterion only needs a set of fracture toughness test data of specimens with any sizes to obtain the FPZ length, and then to predict the K_a of the target configuration. However, as analyzed in Sect. 4.2.1, if the size effect of FPZ is not considered, a large prediction error can be caused. Therefore, it is necessary to select specimens with similar size to the predicted target specimens for fracture test, or to carry out fracture test of multiple groups of specimens with different sizes, to obtain the change rule of FPZ length with specimen size. While in the SEL model, it needs to fit the fracture toughness test data of multiple groups of specimens to obtain the equation for prediction. Compared with the maximum tangential stress fracture criterion, SEL model highlights the integrity and maximizes the use of existing test data, but the workload also increases.

Compared with MTS criterion and MMTS criterion, FIMTS criterion considers more high-order terms to obtain accurate results, which is very important for the prediction of fracture load of small-size specimens. For large-size specimens, MMTS criterion can also obtain sufficient accurate results. In addition, for the fracture of specimens with different configurations, the influence of the number of high-order terms on the prediction results needs to be further studied. In practice, most of the pre-existing cracks in rock masses are often subjected to a combination of tensile and shear loading conditions. When the maximum tangential stress fracture criterion is applied to mixed mode loading conditions, it is necessary to determine the crack initiation angle first, and then determine the tangential stress at the front of the crack tip. Therefore, it is very difficult to determine the high-order term by fitting the tangential stress at the crack tip front through Williams stress expansion. Compared with mode I fracture, the calculation of higher order terms of the specimen in mixed mode loading is more complex, which limits the application of FIMTS criterion to some extent. It is worth noting that the fracture process zone length obtained by mode I fracture results is widely used in the prediction of fracture load in the mixed mode loading (Aliha et al. 2013; Ayatollahi and Akbardoost 2013; Sangsefidi et al. 2020). The crack initiation angle under mixed mode loading is related to the fracture process zone length, and the crack initiation angle and the fracture process zone length jointly determine the fracture load of the specimen. It can be seen that the deviation in determining the fracture process zone length will seriously affect the prediction of the fracture load of the specimen. Therefore, based on the mode I fracture test data of the specimen, the fracture process zone length is determined by FIMTS criterion, and then applied to the prediction of the fracture load of the specimen under the mixed mode loading condition may obtain more accurate prediction results.

5 Conclusion

In this study, the fracture toughness of cracked straight-through Brazilian disc (CSTBD) shale specimens with different sizes was tested. The traditional maximum tangential stress (TMTS) criterion, modified maximum tangential stress (MMTS) criterion, and further improved maximum tangential stress (FIMTS) criterion were used to investigate the change of fracture process zone (FPZ) lengths of specimens with different sizes, and the effective crack model was also used to predict the inherent fracture toughness (K_{Ic}) of the material. Then, the three-point bending fracture tests of notched semi-circular bend (NSCB) specimens were carried out, and the apparent fracture toughness (K_a) was predicted using the above three fracture criteria and the size effect law (SEL) model. The main conclusions are as follows:

(1) With the increase of the specimen size, the K_a and the FPZ lengths obtained by TMTS, MMTS, and FIMTS criteria also increase. For small-size specimens, there is still a large difference between the tangential stress at the front of the crack tip determined by TMTS and MMTS criteria and that determined by finite-element model (FEM). Moreover, with the increase of specimen

size, this gap is decreased gradually, and the difference between the FPZ lengths determined by the MMTS, MTS, and FIMTS criteria is also reduced.

(2) With the FPZ length determined by the FIMTS criterion, the fluctuation of the K_{Ic} predicted by the effective crack model with the specimen size is small, which indicates that the combination of the FIMTS criterion and the effective crack model can better estimate the K_{Ic} of materials.

(3) In the prediction of the K_a of the NSCB specimens, a large prediction error can be caused without considering the size effect of the FPZ. The K_a predicted by the FIMTS criterion is the closest to that obtained by the test, while the K_a predicted by the TMTS and MMTS criteria is quite different from the tested fracture toughness. It indicates that only considering the singular terms or the first three terms of Williams expansion is not enough to accurately describe the fracture behavior of materials.

(4) Based on the failure load of CSTBD specimens with different sizes, the relationship between the configuration size and the failure load is established by the SEL model. However, there is a big deviation when this relationship is used to predict the failure load of NSCB specimens. It shows that the deviation of test data during the establishment of SEL model is easy to affect the prediction results for the configuration in which dimensionless stress intensity factor (Y^*) varies greatly with normalized crack length (α).

Acknowledgements This work was supported by the National Natural Science Foundation of China (Grant no. 42172316), the Natural Science Foundation of Hunan Province (Grant no 2021JJ30810), and the Research Fund of The State Key Laboratory of Coal Resources and Safe Mining, CUMT (SKLCRSM21KF005).

Declarations

Conflict of Interest The authors declare no conflict of interest.

References

Aliha MRM, Ayatollahi MR, Pakzad R (2008) Brittle fracture analysis using a ring-shape specimen containing two angled cracks. Int J Fract 153(1):63–68. https://doi.org/10.1007/s10704-008-9280-9

Aliha MRM, Ayatollahi MR, Smith DJ, Pavier MJ (2010) Geometry and size effects on fracture trajectory in a limestone rock under mixed mode loading. Eng Fract Mech 77(11):2200–2212. https://doi.org/10.1016/j.engfracmech.2010.03.009

Aliha MRM, Sistaninia M, Smith DJ, Pavier MJ, Ayatollahi MR (2012a) Geometry effects and statistical analysis of mode I fracture in guiting limestone. Int J Rock Mech Min Sci 51:128–135. https://doi.org/10.1016/j.ijrmms.2012.01.017

Aliha MRM, Ayatollahi MR, Akbardoost J (2012b) Typical upper bound–lower bound mixed mode fracture resistance envelopes for rock material. Rock Mech Rock Eng 45(1):65–74. https://doi.org/10.1007/s00603-011-0167-0

Aliha MRM, Hosseinpour GR, Ayatollahi MR (2013) Application of cracked triangular specimen subjected to three-point bending for investigating fracture behavior of rock materials. Rock Mech Rock Eng 46(5):1023–1034. https://doi.org/10.1007/s00603-012-0325-z

Ayatollahi MR, Akbardoost J (2013) Size effects in mode II brittle fracture of rocks. Eng Fract Mech 112–113:165–180. https://doi.org/10.1016/j.engfracmech.2013.10.011

Ayatollahi MR, Akbardoost J (2014) Size and geometry effects on rock fracture toughness: mode I fracture. Rock Mech Rock Eng 47(2):677–687. https://doi.org/10.1007/s00603-013-0430-7

Aliha MRM, Ayatollahi MR (2014) Rock fracture toughness study using cracked chevron notched Brazilian disc specimen under pure modes I and II loading—a statistical approach. Theor Appl Fract Mech 69:17–25. https://doi.org/10.1016/j.tafmec.2013.11.008

Aliha MRM, Pakzad R, Ayatollahi MR (2014) Numerical analyses of a cracked straight-through flattened brazilian disk specimen under mixed-mode loading. J Eng Mech 140:219–224. https://doi.org/10.1061/(ASCE)EM.1943-7889.0000651

Aliha MRM (2014) Indirect tensile test assessments for rock materials using 3-D disc-type specimens. Arab J Geosci 7(11):4757–4766. https://doi.org/10.1007/s12517-013-1037-8

Aliha MRM, Bahmani A (2017) Rock fracture toughness study under mixed mode I/III loading. Rock Mech Rock Eng 50(7):1739–1751. https://doi.org/10.1007/s00603-017-1201-7

Aliha MRM, Mahdavi E, Ayatollahi MR (2017) The influence of specimen type on tensile fracture toughness of rock materials. Pure Appl Geophys 174(3):1237–1253. https://doi.org/10.1007/s00024-016-1458-x

Aliha MRM, Mahdavi E, Ayatollahi MR (2018) Statistical analysis of rock fracture toughness data obtained from different chevron notched and straight cracked mode I specimens. Rock Mech Rock Eng 51(7):2095–2114. https://doi.org/10.1007/s00603-018-1454-9

Akbardoost J, Ayatollahi MR, Aliha MRM, Pavier MJ, Smith DJ (2014) Size-dependent fracture behavior of Guiting limestone under mixed mode loading. Int J Rock Mech Min Sci 71:369–380. https://doi.org/10.1016/j.ijrmms.2014.07.019

Akbardoost J (2014) Size and crack length effects on fracture toughness of polycrystalline graphite. Eng Solid Mech 2(3):183–192. https://doi.org/10.5267/j.esm.2014.4.005

Aliha MRM, Mousavi SS (2019) Sub-sized short bend beam configuration for the study of mixed-mode fracture. Eng Fract Mech 225:106830. https://doi.org/10.1016/j.engfracmech.2019.106830

Aliha MRM, Kucheki HG, Asadi MM (2021a) On the use of different diametral compression cracked disc shape specimens for

introducing mode III deformation. Fatigue Fract Eng Mater Struct 44(11):3135–3151. https://doi.org/10.1111/ffe.13570
Aliha MRM, Ebneabbasi P, Reza KarimiNikbakht HE (2021b) A novel test device for the direct measurement of tensile strength of rock using ring shape sample. Int J Rock Mech Min Sci 139:104649. https://doi.org/10.1016/j.ijrmms.2021.104649
Barr B, Hasso E (1986) Fracture toughness testing by means of the SECRBB test specimen. Int J Cem Compos Lightweight Concr 8(1):3–9. https://doi.org/10.1016/0262-5075(86)90019-9
Bazant ZP, Kim JK, Pfeiffer PA (1986) Nonlinear fracture properties from size effect tests. Int J Struct Eng 112(2):289–307. https://doi.org/10.1061/(ASCE)0733-9445(1986)112:2(289)
Bazant ZP, Planas J (1997) Fracture and size effect in concrete and other quasibrittle materials, vol 16. CRC Press, Boca Raton
Bidadi J, Akbardoost J, Aliha MRM (2020) Thickness effect on the mode III fracture resistance and fracture path of rock using ENDB specimens. Fatigue Fract Eng Mater Struct 43(2):277–291. https://doi.org/10.1111/ffe.13121
Bahmani A, Nemati S (2021) Fracture resistance of railway ballast rock under tensile and tear loads. Eng Solid Mech 9(3):271–280. https://doi.org/10.5267/j.esm.2021.3.003
Bahmani A, Farahmand F, Janbaz M, Darbandi A, KuchekiAliha GHMRM (2021) On the comparison of two mixed-mode I + III fracture test specimens. Eng Fract Mech 241:107434. https://doi.org/10.1016/j.engfracmech.2020.107434
China Aviation Academy (1981) Handbook of stress intensity factors. Science Press, Beijing, pp 174–179 **(in Chinese)**
Erdogan F, Sih GC (1963) On the crack extension in plates under plane loading and transverse shear. J Basic Eng. https://doi.org/10.1115/1.3656897
Fowell RJ (1995) ISRM commission on testing methods. Suggested method for determining mode I fracture toughness using cracked chevron notched Brazilian disc (CCNBD) specimens. Int J Rock Mech Min Sci Geomech Abstr 32(1):57–64
Guo H, Aziz NI, Schmidt LC (1993) Rock fracture-toughness determination by the Brazilian test. Eng Geol 33:177–188. https://doi.org/10.1016/0013-7952(93)90056-I
ISRM (1978) Suggested methods for determining tensile strength of rock materials. Int J Rock Mech Min Sci Geomech Abstr 15(3):99–103. https://doi.org/10.1016/0148-9062(78)91494-8
Ju MH, Li JC, Li XF, Zhao JA (2019) Fracture surface morphology of brittle geomaterials influenced by loading rate and grain size. Int J Impact Eng. https://doi.org/10.1016/j.ijimpeng.2019.103363
Kong XM, Schluter N (1995) Effect of triaxial stress on mixed-mode fracture. Eng Fract Mech 52(2):379–388. https://doi.org/10.1016/10.1016/0013-7944(94)00228-A
Karihaloo BL (1999) Size effect in shallow and deep notched quasi-brittle structures. Int J Fract 95:379–390. https://doi.org/10.1023/A:1018633208621
Khan K, Al-Shayea NA (2000) Effect of specimen geometry and testing method on mixed mode I–II fracture toughness of a limestone rock from Saudi Arabia. Rock Mech Rock Eng 33(3):179–206. https://doi.org/10.1007/s006030070006
Kuruppu MD (1997) Fracture toughness measurement using chevron notched semi-circular bend specimen. Int J Fract 86:33–38. https://doi.org/10.1023/A:1007426001582
Keles C, Tutluoglu L (2011) Investigation of proper specimen geometry for mode I fracture toughness testing with flattened Brazilian disc method. Int J Fract 69:61–75. https://doi.org/10.1007/s10704-011-9584-z
Kuruppu MD, Obara Y, Ayatollahi MR, Chong KP, Funatsu T (2014) ISRM-suggested method for determining the mode I static fracture toughness using semi-circular bend specimen. Rock Mech Rock Eng 47:267–274. https://doi.org/10.1007/s00603-013-0422-7
Liu XL, Liu Z, Li XB, Gong FQ, Du K (2020) Experimental study on the effect of strain rate on rock acoustic emission characteristics. Int J Rock Mech Min Sci 133:104420. https://doi.org/10.1016/j.ijrmms.2020.104420
Mahdavi E, Aliha MRM, Bahrami B, Ayatollahi MR (2020) Comprehensive data for stress intensity factor and critical crack length in chevron notched semi-circular bend specimen subjected to tensile type fracture mode. Theor Appl Fract Mech 106:102466. https://doi.org/10.1016/j.tafmec.2019.102466
Nallathambi P, Karihaloo BL (1987) Determination of specimen-size independent fracture toughness of plain concrete. Mag Concr Res 38(135):67–76. https://doi.org/10.1680/macr.1987.39.139.113
Ouchterlony F (1988) ISRM commission on testing methods. Suggested methods for determining fracture toughness of rock. Int J Rock Mech Min Sci Geomech Abstr 25:71–96
Sih GC (1974) Strain energy density factor applied to mixed mode crack problems. Int J Fract 10(3):305–321. https://doi.org/10.1007/BF00035493
Smith DJ, Ayatollahi MR, Pavier MJ (2010) The role of T-stress in brittle fracture for linear elastic materials under mixed-mode loading. Fatigue Fract Eng Mater Struct 24(2):137–150. https://doi.org/10.1046/j.1460-2695.2001.00377.x
Sangsefidi M, Akbardoost J, Mesbah M (2020) Experimental and theoretical fracture assessment of rock-type U-notched specimens under mixed mode I/II loading. Eng Fract Mech 230:106990. https://doi.org/10.1016/j.engfracmech.2020.106990
Sangsefidi M, Akbardoost J, Zhaleh AR (2021) Assessment of mode I fracture of rock-type sharp V-notched samples considering the size effect. Theor Appl Fract Mech 116:103136. https://doi.org/10.1016/j.tafmec.2021.103136
Tutluoglu L, Karatas Batan C, Aliha MRM (2022) Tensile mode fracture toughness experiments on andesite rock using disc and semi-disc bend geometries with varying loading spans. Theor Appl Fract Mech 119:103325. https://doi.org/10.1016/j.tafmec.2022.103325
Williams ML (1957) On the stress distribution at the base of a stationary crack. J Appl Mech 24:109–114. https://doi.org/10.1115/1.4011454
Wei MD, Dai F, Xu NW, Liu Y, Zhao T (2017) A novel chevron notched short rod bend method for measuring the mode I fracture toughness of rocks. Eng Fract Mech 190:1–15. https://doi.org/10.1016/j.engfracmech.2017.11.041
Wei MD, Dai F, Zhou JW, Yi L, Jin L (2018) A further improved maximum tangential stress criterion for assessing mode I fracture of rocks considering non-singular stress terms of the williams expansion. Rock Mech Rock Eng 51:3471–3488. https://doi.org/10.1007/s00603-018-1524-z
Xu Y, Dai F, Xu NW, Zhao T (2016) Numerical investigation of dynamic rock fracture toughness determination using a semi-circular bend specimen in split Hopkinson pressure bar testing. Rock Mech Rock Eng 49(3):731–745. https://doi.org/10.1007/s00603-015-0787-x
Xie Q, Li SX, Liu XL, Gong FQ, Li XB (2020) Effect of loading rate on fracture behaviors of shale under mode I loading. J Cent South Univ 27(10):3118–3132. https://doi.org/10.1007/s11771-020-4533-5
Zhang QB, Zhao J (2013) Effect of loading rate on fracture toughness and failure micromechanisms in marble. Eng Fract Mech 102:288–309. https://doi.org/10.1016/j.engfracmech.2013.02.009
Zhou ZL, Cai X, Ma D, Du X, Chen L, Wang HQ, Zang HZ (2018) Water saturation effects on dynamic fracture behavior of sandstone. Int J Rock Mech Min Sci 114:46–61. https://doi.org/10.1016/j.ijrmms.2018.12.014